Electronic Supplementary Material (ESI) for Energy & Environmental Science.
This journal is © The Royal Society of Chemistry 2015

Supplementary Information

An Order/Disorder/Water Junction System for Highly Efficient Co-Catalyst-Free Photocatalytic Hydrogen Generation

Kan Zhang,[a†] Luyang Wang,[b†] Jung Kyu Kim,[c] Ming Ma,[c] Ganapathy Veerappan,[c] Chang-Lyoul Lee,[d] Ki-jeong Kong,[e]
Hyoyoung Lee [bc*] and Jong Hyeok Park[a*]

Materials and Methods
Supplementary Text
Figures S1-S15
Full References (*1-13*)

Materials and Methods

Experimental details.14 mg metallic Li foil was dissolved in 20 ml ethanediamine to form a 1mmol/ml solvated electron solution. 200 mg dried TiO_2 nanocrystals (anatase, size: ~25 nm, rutile, size: ~140 nm, P-25, size: 20~40 nm) were added into above solution and stirred for 6 days (Caution: the reaction needs to be performed in closed and anhydrous condition). After sufficient reaction, 1 mol/L HCl was slowly dropped into the mixture to order to quench the excess electrons and form Li salts. Finally, the resulting composite was rinsed by deionized water several times, and dried at room temperature in vacuum oven.

Photocatalysts loaded with Pt was obtained by photo-deposition method. The photocatalytic H_2 evolution experiments were performed in a 100 mL Pyrex round-bottom flask, the openings of which were sealed with a silicone rubber septum, at ambient temperature and atmospheric pressure. A solar simulator (Oriel Sol 3A, class AAA) with a filtered 450 W xenon lamp was employed as the light source, and proper adjustments were made with a Si reference cell (VLSI standards, Oriel P/N 91150 V) in order to produce a 1 sunlight intensity of 100 mW/cm^2. In a typical experiment, 20 mg of the photocatalyst was dispersed in a mixture of 35 mL water and 35 mL of methanol. The suspension was bubbled with nitrogen to ensure almost removal of dissolved oxygen. During the photocatalysis, the suspension was continuously stirred to ensure uniform irradiation. A 1mL sample of the generated gas was collected using a glass injection syringe which could be sealed up and hydrogen and oxygen content was analyzed by gas chromatograph (Agilent technologies 7890A GC system, USA). To evaluate the H_2 production rate/cm^2, the reactor was covered to 1 cm^2 area using black foam with a thickness of 0.5 cm.

Time-Correlated Single Photon Counting (TCSPC) was performed to measure the exciton lifetimes (charge dissociation efficiency). The second harmonic (SHG = 375 nm) of a tunable Ti:sapphire laser (Mira900, Coherent) with ~150 fs pulse width and 76 MHz repetition rate was used as an excitation source. The PL emission was spectrally resolved by using some collection optics and a monochromater (SP-2150i, Acton). The TCSPC module (PicoHarp, PicoQuant) with MCP-PMT (R3809U-59, Hamamatsu) was used for ultrafast detection. The total instrument response function (IRF) was less than 130 ps, and the temporal time resolution was less than 10 ps. The deconvolution of actual fluorescence decay and IRF was performed by using a fitting software (FlouFit, PicoQuant) to deduce the time constant associated with each exponential decay. All measurements were performed under vacuum at 20K. Low temperature photoluminescence (fs-PL) is measured by using collection optics and a monochromator (SP-2150i, Acton) connected with a photomultiplier tube (PD-174, Acton).

Computational details

We performed spin-polarized ab initio periodic calculations using the Vienna ab initio Simulation Package (VASP) code.[1,2] In the VASP program, the Kohn–Sham equations are solved using the generalised gradient approximation (GGA) proposed by Perdew, Becke and Ernzerhof.[3] The interactions between the atomic core ions and the valence electrons are approximated by the frozen-core projector-augmented wave (PAW) pseudopotentials.[4] Convergence of the total energy was achieved by setting the plane-wave cutoffs for the wave function expansion and the charge density to 400 and 800 eV, respectively.

The computational models

For the bulk rutile structure, we used a 2 × 2 × 3 supercell with 72 atoms. The dimensions of the supercell were 9.188 × 9.188 × 8.877 Å^3. For the bulk anatase structure, we used a supercell with 108 atoms (i.e., 3 × 3 × 1). The optimized bulk lattice parameters were a = 3.776 Å and c = 9.486 Å. The integrations in the Brillouin zone were performed on a grid of 4 × 4 × 4 Monkhorst–Pack set. The total energies converged to 10^{-6} eV. All structures were fully optimized, with the largest residual force being smaller than 0.01 eV/Å.

For a supercell, the defect formation energy is defined as

$$E_f(\mathrm{Vac}) = E(\mathrm{TiO}_{2-x}) - E(\mathrm{TiO}_2) - E(\tfrac{1}{2}\mathrm{O}_2)$$

where $E(TiO_{2-x})$ is the total energy of defective TiO_2 and $E(TiO_2)$ is the total energy of the supercell without the defect. The chemical potential of dopant O is referenced to the energy of oxygen in an isolated O_2 molecule, calculated to be -4.93 eV.

The equilibrium bulk geometry was used to construct surfaces with slab geometries. These slabs were separated from their periodic images normal to the surface by a vacuum gap of about 20 Å, to give a pseudo-2D periodic system. All the surface slabs have sufficiently large lateral dimension (surface area 153.8 and 115.7 Å^3 for rutile (110) and anatase (101) surface, respectively) to neglect artificial interaction from the size limitation. For the **k**-space integration, Monkhorst-Pack point sampling of 4 × 4 × 1 was used, where the third reciprocal vector is aligned with the surface normal. Initial geometric relaxations were performed for each of the stoichiometric surfaces, in which all the atoms were allowed to move freely, and the minimization was deemed to be converged when the forces on each ion were smaller than 0.01 eV Å^{-1}. After the stoichiometric surfaces had been relaxed, a single oxygen atom was removed from both surfaces of each slab, ensuring that an artificial dipole was not created perpendicular to the slab. These reduced slabs were then relaxed further, using the same convergence criteria. In order to avoid the interaction between defects in each side, we have used sufficiently thick slabs, 10 TiO_2 layer for rutile (110) surface and 8 layer for anatase (101) surface.

In VASP modeling of the surface properties, the dipole correction, proposed by Neugabeauer and Scheffler,[5] was used. The correction removes the artificial filed arising in the empty space from the use of Periodic Boundary Conditions (PBC) in solution of Poisson equation by Fast Fourier Transform (FFT) method. The dipole in the slab is compensated by artificial dipole layer located in the empty space.

Solid-state NMR measurements:

Solid-state NMR probe with a 4 mm stator assembly from Solid 400MHz WB NMR (Bruker AVANCE 400WB, Biospin). The magic angle spinning (MAS) rate was 14 kHz.

XPS and VB XPS measurements:

X-ray photoelectron spectroscopy (XPS) measurements were recorded by AESXPS instrument (ESCA2000 from VG Microtech in England) equipped with an aluminum anode (Al Kα = 1486.6 eV).

UV-vis absorption measurements:

UV-vis diffuse reflectance spectra were recorded using a UV−vis spectrophotometer (Shimadzu UV-3600 Japan) using $BaSO_4$ as a reference at room temperature.

Apparent quantum efficiency evaluation

$$\text{(Apparent quantum efficiency (QE\%)} = \frac{Number\ of\ reacted\ electrons}{Number\ of\ incident\ photons} \times 100\% = \frac{2 \times Number\ of\ evolved\ H_2\ molecules}{Number\ of\ incident\ photons} \times 100\%$$

Supplementary Text

[Simulation result 1]

In order to elucidate why rutile phase was easily reduced compared to anatase phase, we have computed the formation energy of the oxygen vacancy with respect to $\frac{1}{2}O_2$; [$E_f(Vac) = E(TiO_{2-x}) - E(TiO_2) - E(\frac{1}{2}O_2)$] for x = 0.028 (rutile) and 0.021 (anatase). The liquid-solid interface (TiO_2 and Li-EDA) was considered as reaction sites. The calculated formation energies E_f(Vac) at anatase (101) surface and rutile (110) surface were 3.95 eV and 3.51 eV, respectively. The smaller E_f(Vac) indicates the more reducible the system. The formation energies E_f(Vac) changes versus pH are estimated by considering surface adsorbability of (H^+ or OH^-). According to the Gouy-Chapman theory, the surface potential (Ψ) can be calculated from the surface charge density (σ).[6,7]

$$\Psi = \frac{2kT}{ze} asinh\left(\frac{\sigma}{\sqrt{8n\epsilon kT}}\right)$$

Where k is the Boltzmann's constant, T is the temperature, z is the value of the valance of the ions (for 1:1 one, *z*=1), *e* is the electron charge (1.602×10^{-19} C), n is the concentration of the electrolyte, and ϵ is the dielectric constant. Comparison E_f(Vac) of anatase and rutile versus pH are shown below.

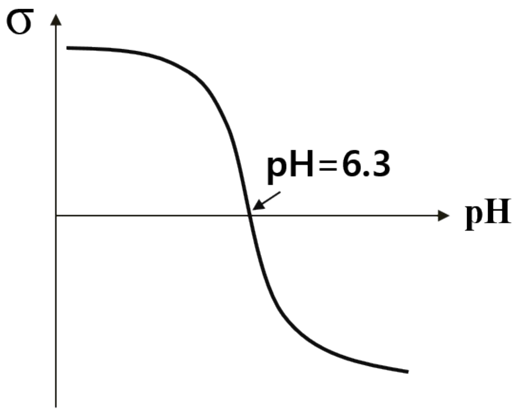

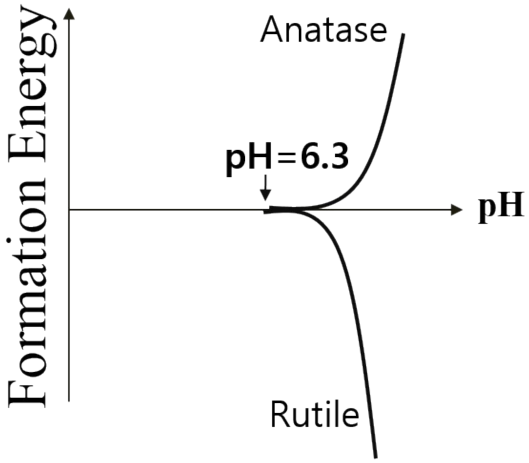

[Simulation result 2]

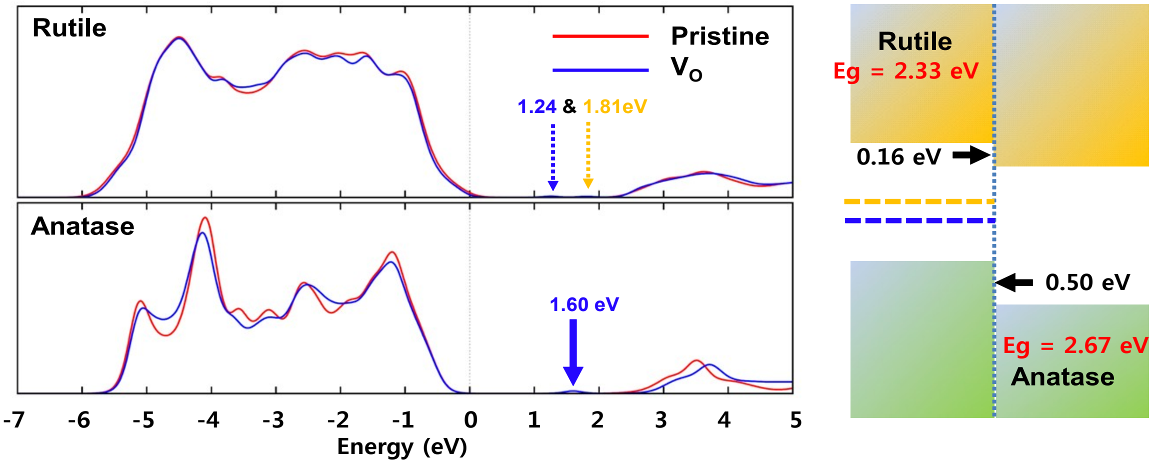

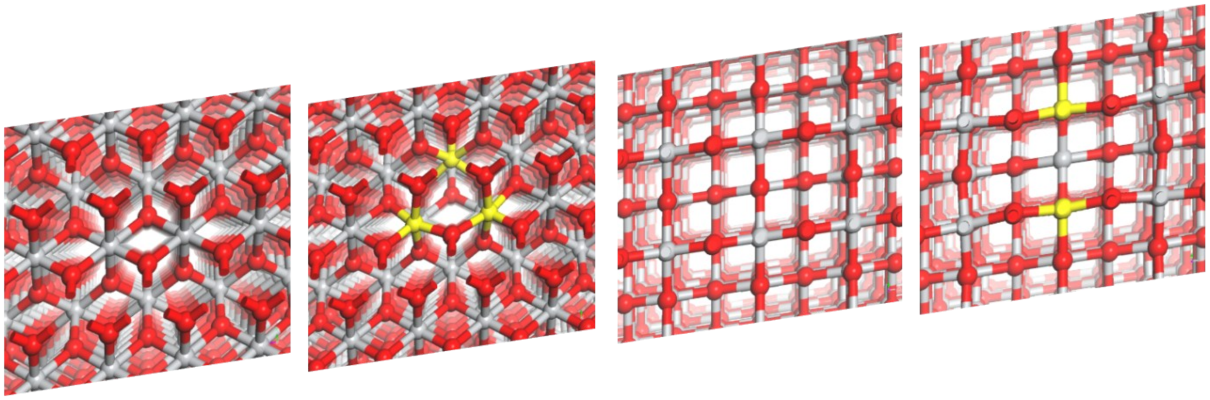

From left to right: Schematic of the supercell adopted for modelling the TiO_2 surface (grey, Ti atoms; red, O atoms; yellow, dangling Ti atoms). A (110)-faceted rutile crystal. A disordered (110)-faceted rutile crystal. A (101)-faceted anatase crystal. A disordered (101)-faceted anatase crystal.

We show the electronic density of states (DOS) with Gaussian broadening of 0.1 eV for rutile and anatase. In this case, the simulation results could reveal the existence of type-II band alignment between reduced rutile phase and pure anatase phase. The calculated bandgaps are 2.33 eV in rutile and 2.67 eV in anatase. Although the values are somewhat smaller than experimental ones (3.04 and 3.42 eV, respectively) *(24)*, the difference between two bandgaps agrees well. Because there exists an ambiguity of energy reference in pseudopotential method, we aligned the energy levels of each phases by comparing the deep-lying Ti 3*p* orbital level. From DOS calculations we conclude that the bulk conduction band edge of rutile lies 0.16 eV above that of anatase, while the VB offset is 0.50 eV. For the slab calculations, we have used the most stable surface in each phase, (110) surface for rutile and (101) surface for anatase. The slab thicknesses (vacuum thicknesses) are 12.80 Å (22.20 Å) and 16.98 Å (19.02 Å) for rutile and anatase respectively. The calculated bandgaps become slightly larger than their bulk values, 2.67 eV and 2.75 eV for rutile (110) surface and anatase (101) surface, respectively. The valence band edge calculated with reference to the vacuum energy level is -6.38 eV for rutile (110) surface and -6.68 eV for anatase (101) surface. The conduction band edge of rutile (110) surface is 0.12 eV higher than anatase (101) surface.

Table S1. PL lifetimes and fractional intensities of P-25 and R-TiO_2 crystal films with and without disordering[a].

Sample name	$\tau_1(f_1)$/ns	$\tau_2(f_2)$/ns	τ_{avr}/ns[b]	χ^{2}[c]
P-25	0.28 (0.71)	2.16 (0.29)	0.83	0.969
Blue P-25	0.19 (0.85)	1.87 (0.15)	0.44	1.010
R-TiO_2	0.14 (0.90)	2.37 (0.10)	0.36	1.015
Black R-TiO_2	0.28 (0.81)	1.94 (0.19)	0.59	0.981

[a]The monitored wavelength was 430 (P-25, R-TiO_2 and black R-TiO_2) and 440nm (blue P-25). The PL decay curves were fitted to a bi-exponential function to calculate the lifetime of the samples. [b]The amplitude-weighted average exciton lifetime (τ_{avr}) was $f_1\tau_1 + f_2\tau_2$, where f_1 and f_2 are fractional intensities and τ_1 and τ_2 are lifetimes. [c]χ^2 is the reduced chi-square value.

Table S2. Summarisation of various coloured TiO_2 photocatalysts for their H_2 evolution behavior recently.

Photocatalyst	Structure	Photocatalysis parameters	H_2 generation rate	The turnover number (TON)	Reference
Hydrogenated anatase TiO_2	Core/shell	0.6 wt.% Pt loading in 1:1 methanol/H_2O	~10 mmol/h/g	325080	Science. 2011. 331. 746-750
Hydrogenated P-25	Core/shell	1 wt.% Pt loading in 1:4 methanol/H_2O	3.94 mmol/h/g	1537	RSC Adv., 2014, 4, 1128–1132
Hydrogenated ordered mesoporous anatase TiO_2	Core/shell	1 wt.% Pt loading in 1:4 methanol/H_2O	1.362 mmol/h/g	2657	J. Am. Chem. Soc. 2014, 136, 9280−9283
Anatase TiO_2 by Al reduction	Core/shell	0.5 wt.% Pt loading in 1:4 methanol/H_2O	7.4 mmol/h/g	28872	Energy Environ. Sci., 2014, 7, 967–972
Hydrogenated anatase TiO_2	Core/shell	1 wt.% Pt loading in 1:4 methanol/H_2O	2.15 mmol/h/g	41935	Chem. Commun., 2012, 48, 5733.
Hydrogenated P-25	Core/shell	1 wt.% Pt loading in 1:4 methanol/H_2O	7.744 mmol/h/g	151045	Chem. Commun., 2014, 50, 6049.
Hydrogenated anatase TiO_2	Core/shell	0.5 wt.% Pt loading in 1:4 methanol/H_2O	8.2 mmol/h/g	319878	Adv. Funct. Mater., 2013, 23, 5444.
Rutile TiO_2 by Zn reduction	Core/shell	1 wt.% Pt loading in 30 vol% methanol/H_2O	~6 mmol/h/g	126805	Chem. Commun., 2014, 50, 2755-2757
$NaBH_4$ reduced P-25	Core/shell	1 wt.% Pt loading in 1:4 methanol/H_2O	6.5 mmol/h/g	126781	Nanoscale, 2014, 6, 10216-10223
Li-EDA treated P-25	**Heterojunction**	**0.5 wt.% Pt loading in 1:1 methanol/H_2O**	**13.89 mmol/h/g**	541943	**Our work**
Hydrogenated anatase TiO_2	Core/shell	No Pt loading in 1:1 methanol/H_2O	3.25 μmol/h/cm^2		Nano Lett. 2014, 14, 3309−3313
Hydrogenated anatase TiO_2 nanotube	Core/shell	No Pt loading in 1:1 methanol/H_2O	7 μmol/h/cm^2		Nano Lett. 2014, 14, 3309−3313
Li-EDA treated P-25	**Heterojunction**	**No Pt loading in 1:1 methanol/H_2O**	**12.86 μmol/h/cm^2 (3.46 mmol/g/h)**		**Our work**

The turnover number (TON) per hour was calculated by using the following formula; TON = moles of H_2 molecules evolved/moles of active sites (Pt on the photocatalyst),

$$TON = \frac{moles\ of\ H_2\ evolved/h}{moles\ of\ Pt\ on\ photocatalyst}$$

In our case, the H_2 generation ratio was 13.89 mmol/g/h and the photocatalyst dosage was 20 mg, the H_2 evolution rate could be calculated to be 0.2778 mmol/h.

The 0.5 wt.% Pt was loaded on 20 mg photocatalyst, the moles of Pt could be calculated to be 5.126×10^{-7} mole.

Thus, $TON = \frac{0.2778}{5.126 \times 10^{-7}}$ = 541943.

Compared to core/shell structure, the higher TON of blue P-25 could be considered there are additional active sites from the order/disorder/water junction for H_2 evolution, which seems to be responsible for high co-catalyst free H_2 generation.

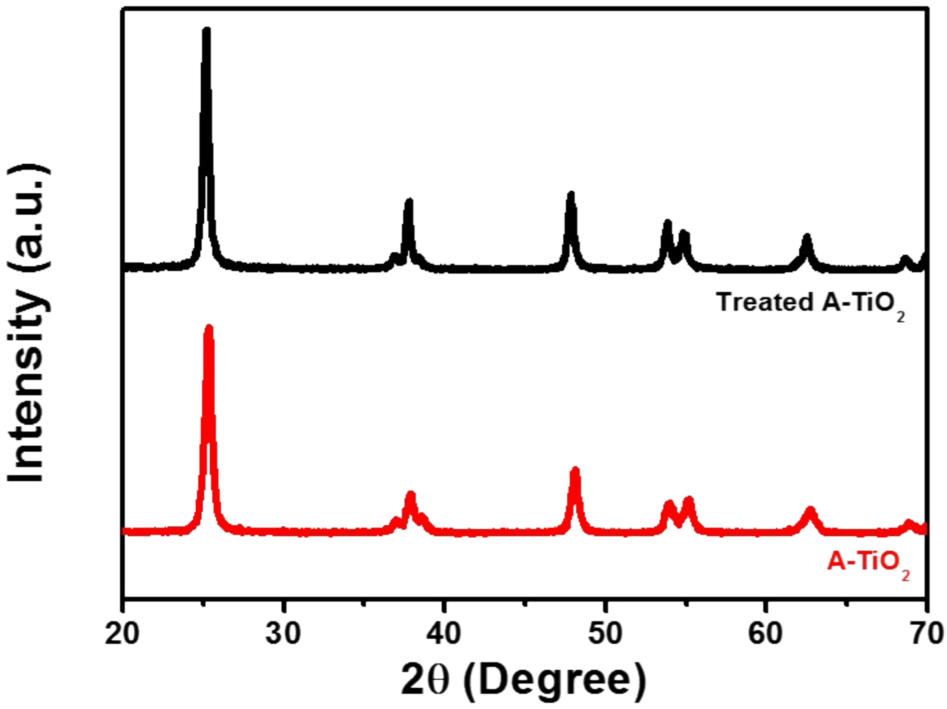

Figure S1. XRD patterns of A-TiO$_2$ crystals and the Li-EDA treated A-TiO$_2$ for 6 days.

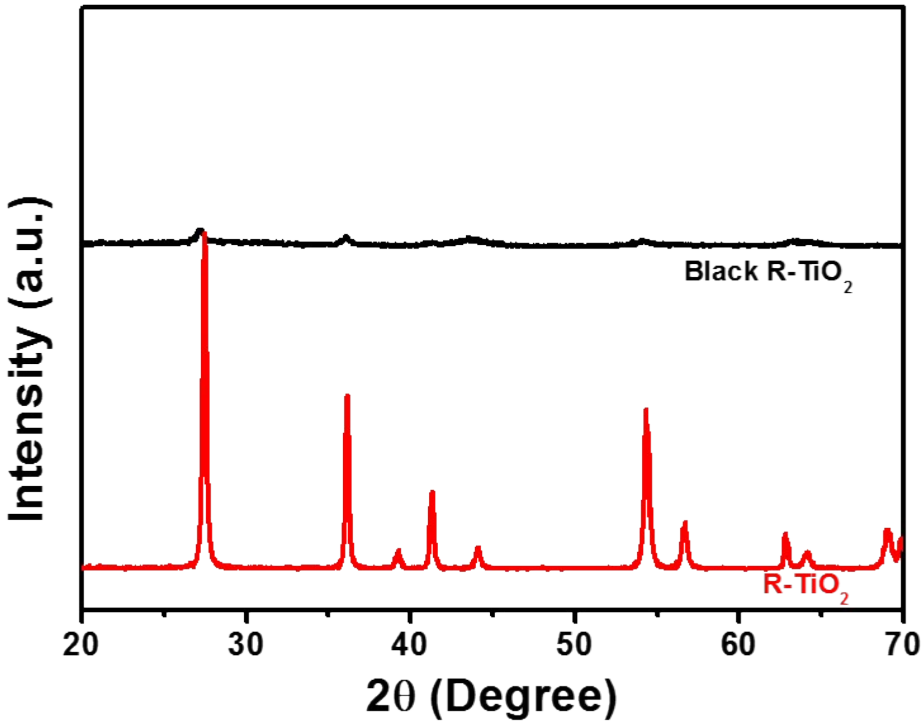

Figure S2. XRD patterns of R-TiO_2 crystals and the Li-EDA treated R-TiO_2 for 6 days.

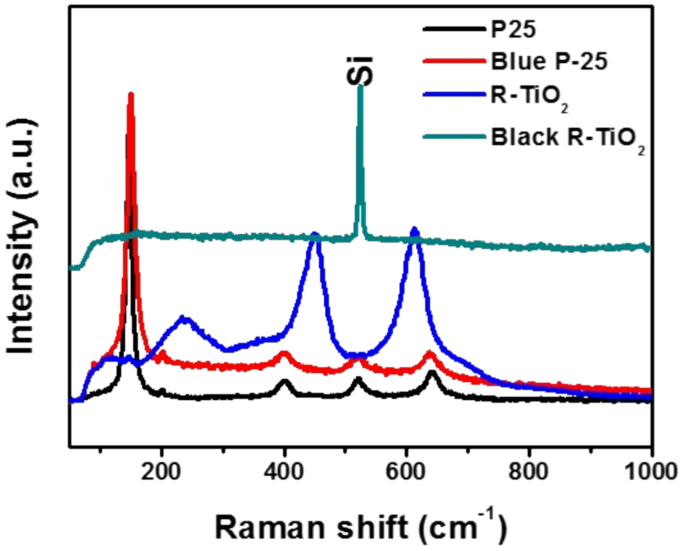

Figure S3. Raman spectra of P-25, blue TiO_2, R-TiO_2 and black R-TiO_2.

The Raman spectra of P-25 and blue P-25 showed five clear bands at 149, 400, 520 (a doublet) and 637 cm^{-1}, which were assigned to the fundamental E_g, B_{1g}, A_{1g}&B_{2g} and E_{2g} modes of anatase, while rutile has two active modes (B_{1g}, B_{2g}) situated at 448 and 612 cm^{-1}, which were completely disappearance.[9]

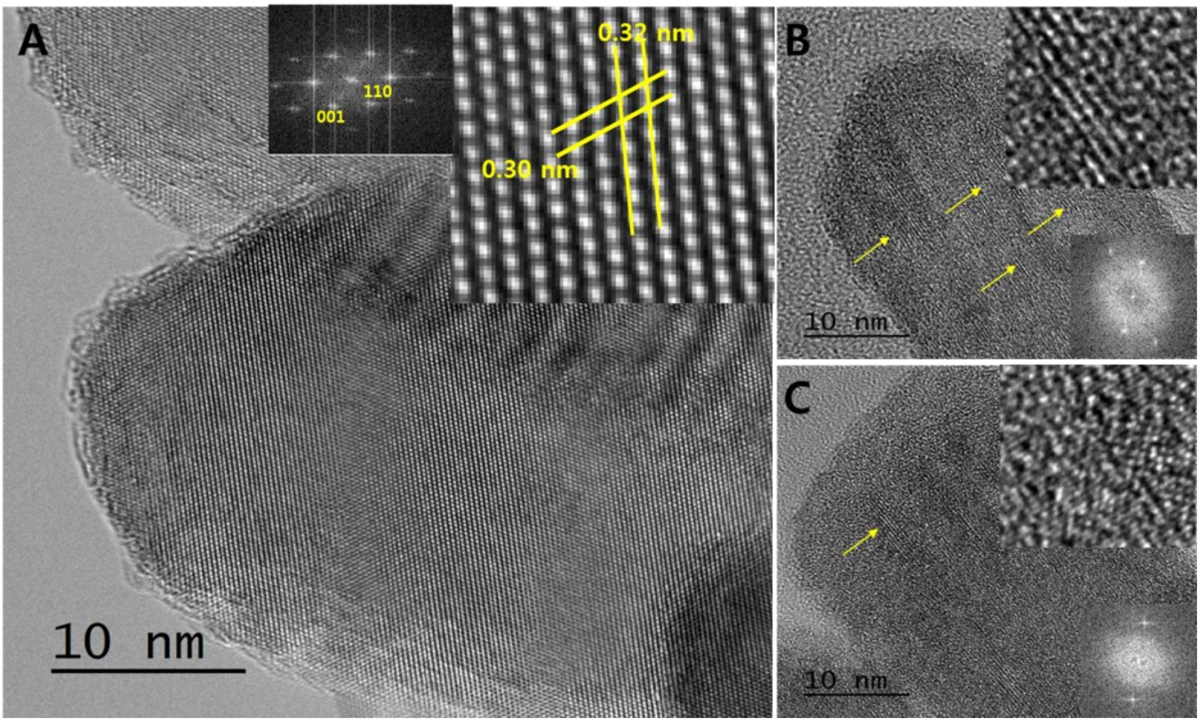

Figure S4. HR-TEM of R-TiO_2 (A), the Li-EDA treated for 20h (B), and the black rutile TiO_2 by Li-EDA treatment for 6days (C).

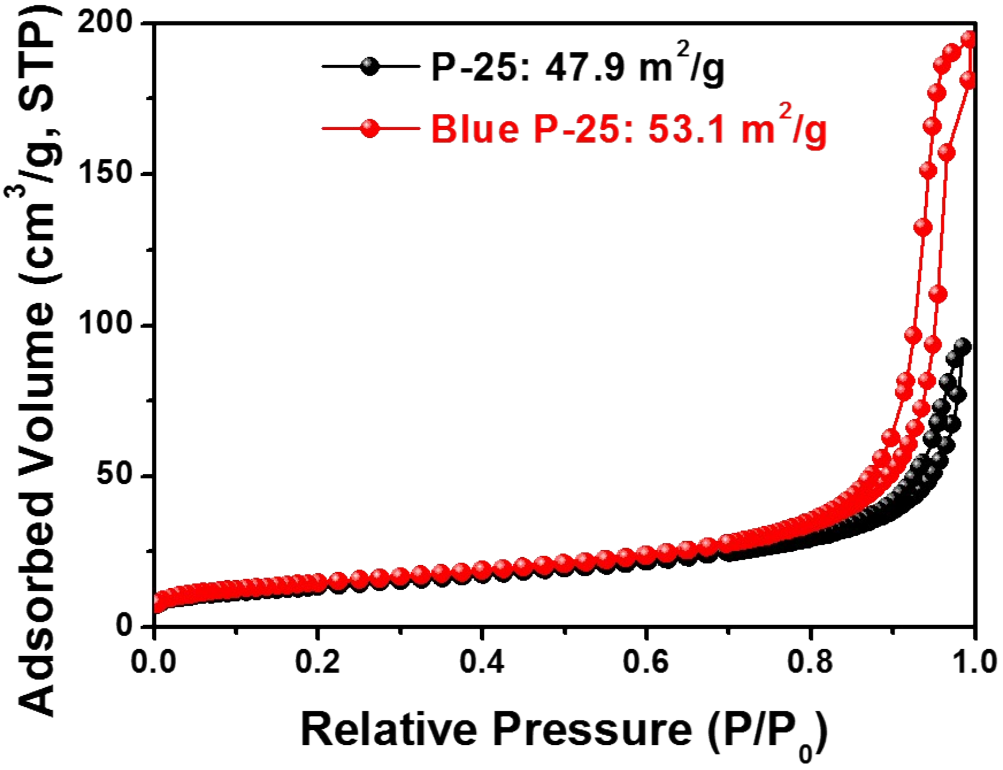

Figure S5. BET surface area of the P-25 and blue P-25.

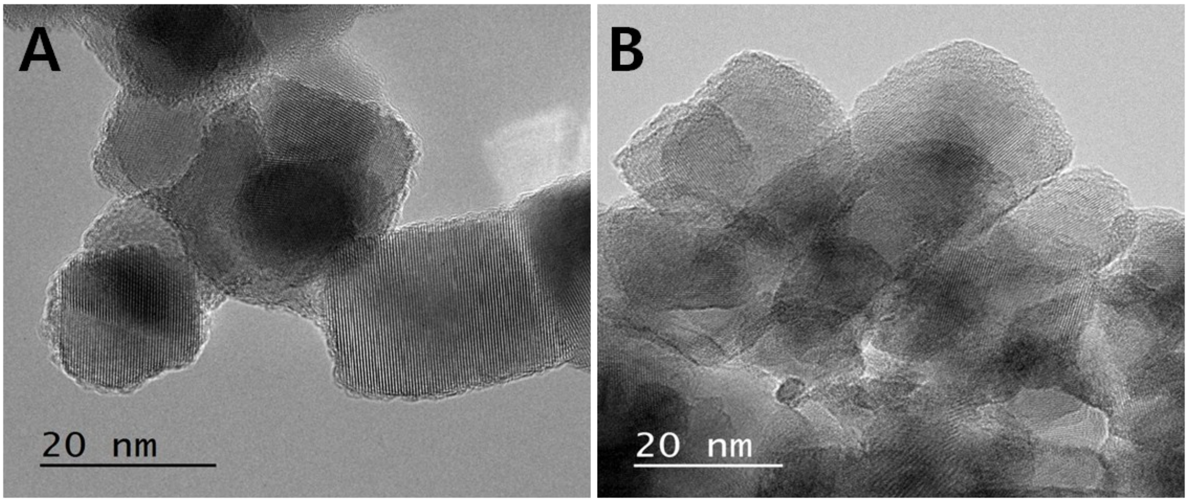

Figure S6. TEM images of the P-25 (A) and blue P-25 (B).

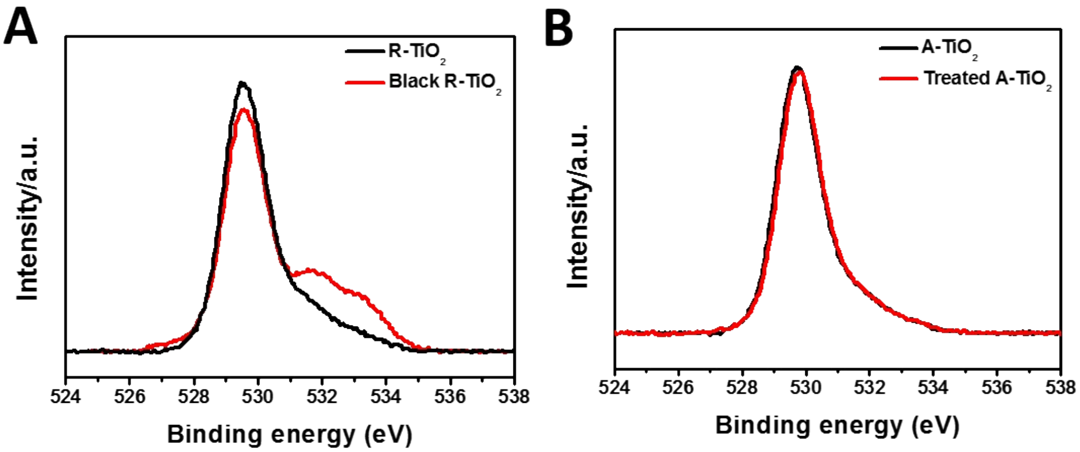

Figure S7. Comparison of O1s XPS spectra of the rutile TiO_2 and black R-TiO_2 (A), original anatase TiO_2 and Li-EDA treated A-TiO_2 (B).

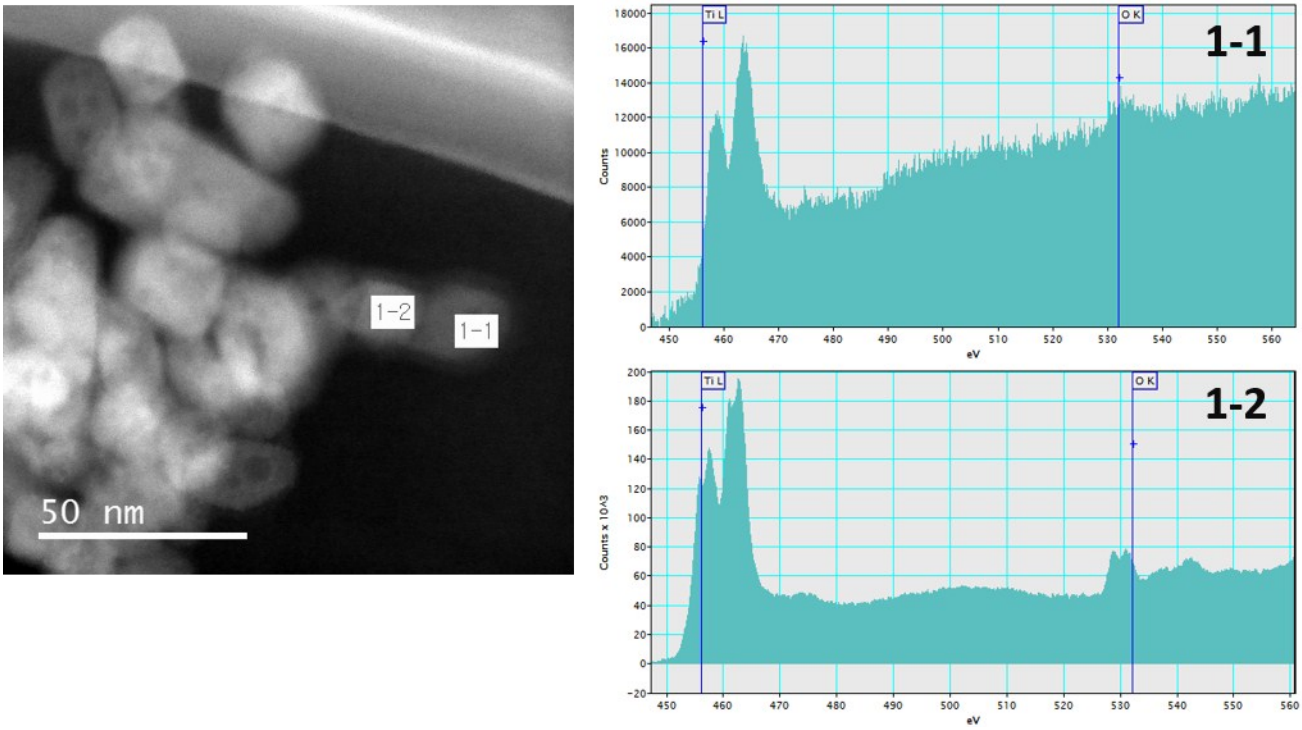

Figure S8. TEM image and the corresponding EELS spectra obtained at the points indicated.

The EELS of Ti-L and O-K at the rectangular region showed that oxygen is deficient in named “1-1” point compared to named “1-2” point. The EELS results clearly showed that oxygen vacancies are selectively generated in R-TiO_2 according to XPS analysis.

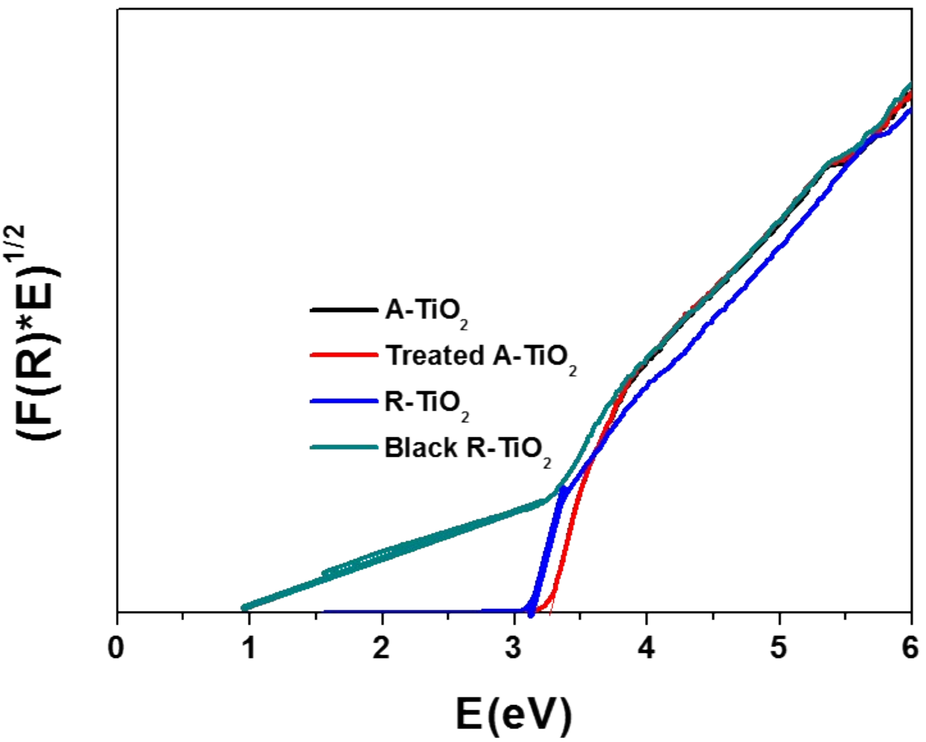

Figure S9. The plot of transformed Kubelka-Munk function versus the energy of light.

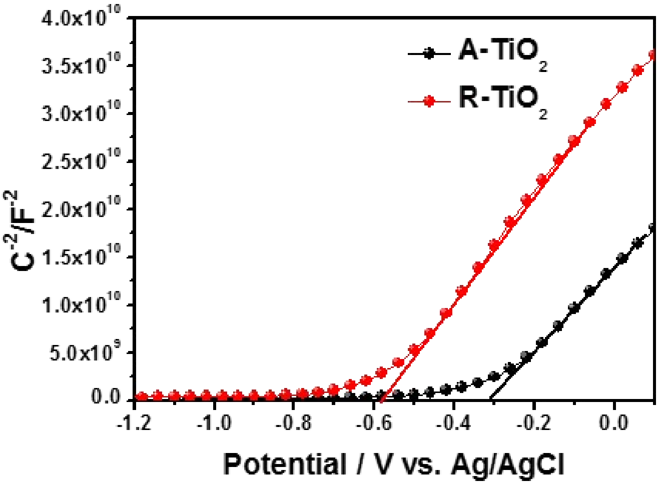

Figure S10. Mott–Schottky plots of the A-TiO_2 and R-TiO_2 measured at a frequency of 1 kHz.

The Mott−Schottky plots were measured in 1M NaOH (pH≈14) electrolyte. The flat band potentials (E_{fb}) of A-TiO_2 and R-TiO_2 samples are estimated to be -0.31 and -0.58 V vs. Ag/AgCl, respectively. The measured potential vs. Ag/AgCl could be converted to the reversible hydrogen electrode (RHE) scale via the Nernst equation:

$$E\ (\text{vs. RHE}) = V_{fb} + E\text{Ag/AgCl (reference)} + 0.0591 \times \text{pH}$$

$$E\text{Ag/AgCl (reference)} = 0.1976 \text{ vs. NHE at } 25\ ^\circ\text{C}$$

Therefore, E_{fb} of A-TiO_2 and R-TiO_2 samples are estimated to be -0.47 and -0.65 V vs. RHE, respectively.

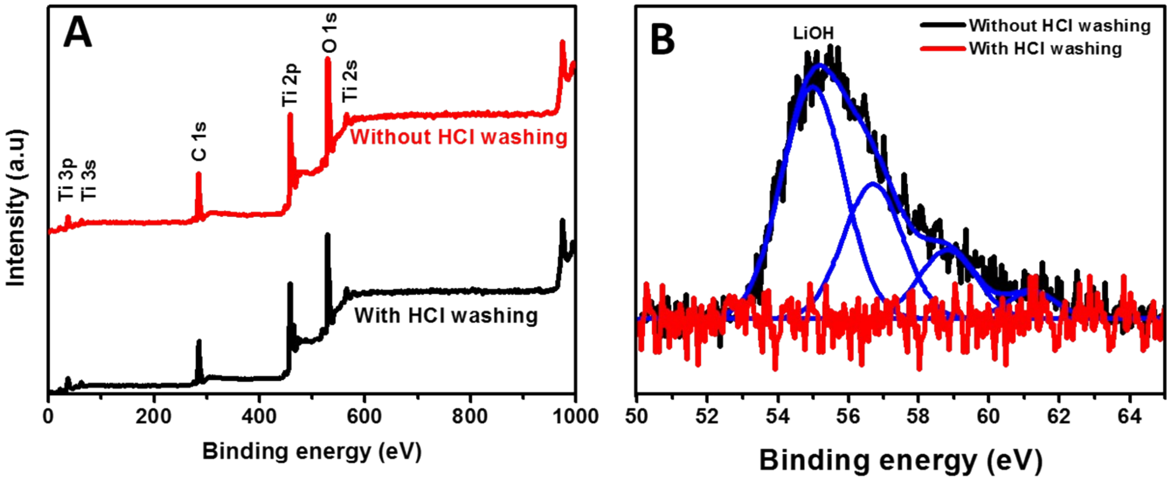

Figure S11. (a) Full XPS spectra of blue P-25 with/without HCl washing. (b) Deconvolution of Li 1s spectra of blue P-25 with/without HCl washing.

Obvious Li impurities were remained in blue P-25 without HCl washing. Binding energy at 54.9 eV could be assigned to LiOH, while other peaks higher than 54.9 eV might be due to some electron withdrawing groups. The EDA superbase given a high pH condition for weakening rutile TiO_2 stability, which means the Gibbs free energy of Rutile is improved dramatically. When reacted with strong reducing agent derived by the chelate metallic Li, lower bond energy of Ti-O in rutile TiO_2 could be break up. The unsaturated bonds in disordered TiO_2 lead to high affinity with proton. Therefore, with washed with diluted HCl, the proton could be introduced into disordered TiO_2 to form Ti-H or Ti-OH bonds.

1) O-Ti-O-Ti-O-Ti-O + e- → ···O-Ti + O-Ti-O-Ti-O···
2) ···O-Ti + O-Ti-O-Ti-O··· + H →···O-Ti-H + HO-Ti-O-Ti-O···

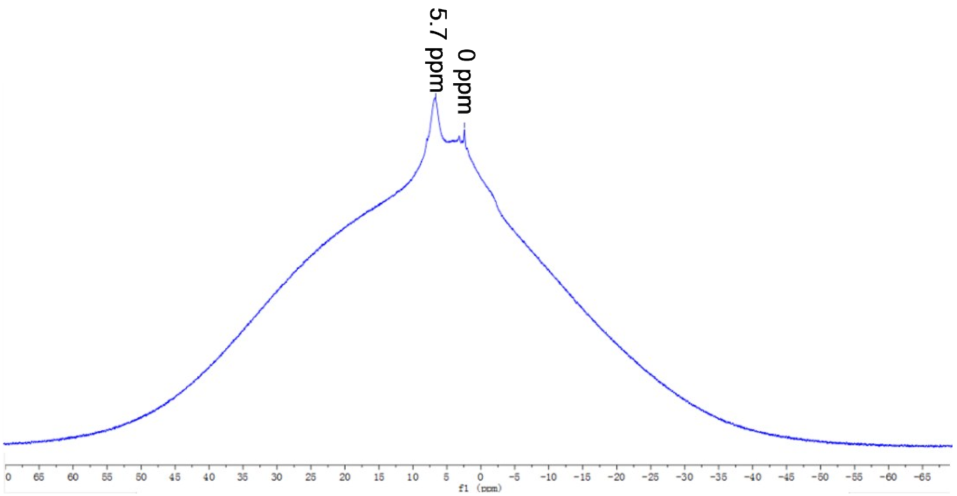

Figure S12. ^{1}H solid NMR spectra of black R-TiO_2.

A strong peak is observed for the protons at 5.7 ppm, which is probably associated with removal of crystallographic water and (to a smaller extent) with physically adsorbed water molecules.[10,11] A peak around 0 ppm were attributed to the presence of interstitial hydrogen with a high dynamic exchange between hydrogen.[12] Another small peak located at 2.4 ppm, which is probably associated with surface OH groups.[13]

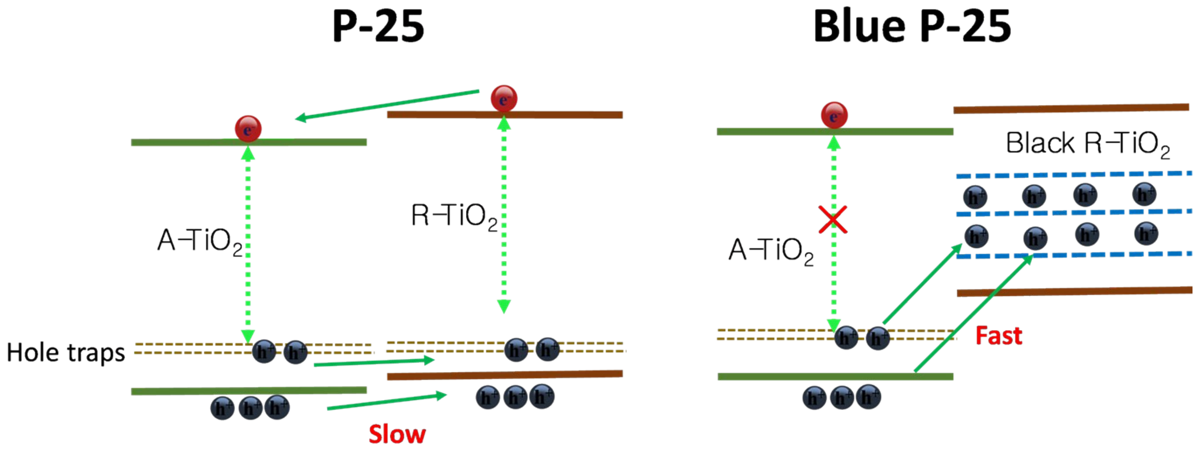

Figure S13. Schematic illustration of reduced charge recombination in the order/disorder/water junction.

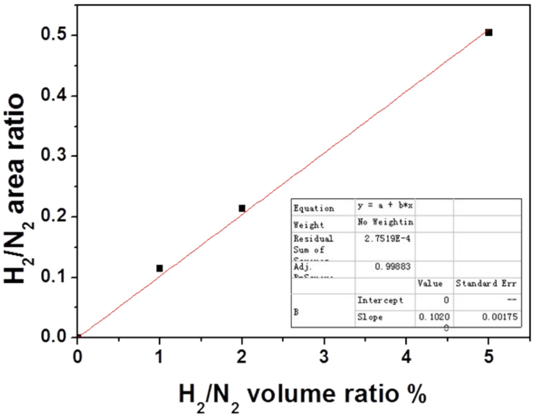

Figure S14. The base of verification using standard 1 vol%, 2 vol% and 5 vol% H_2/N_2 mixed gas.

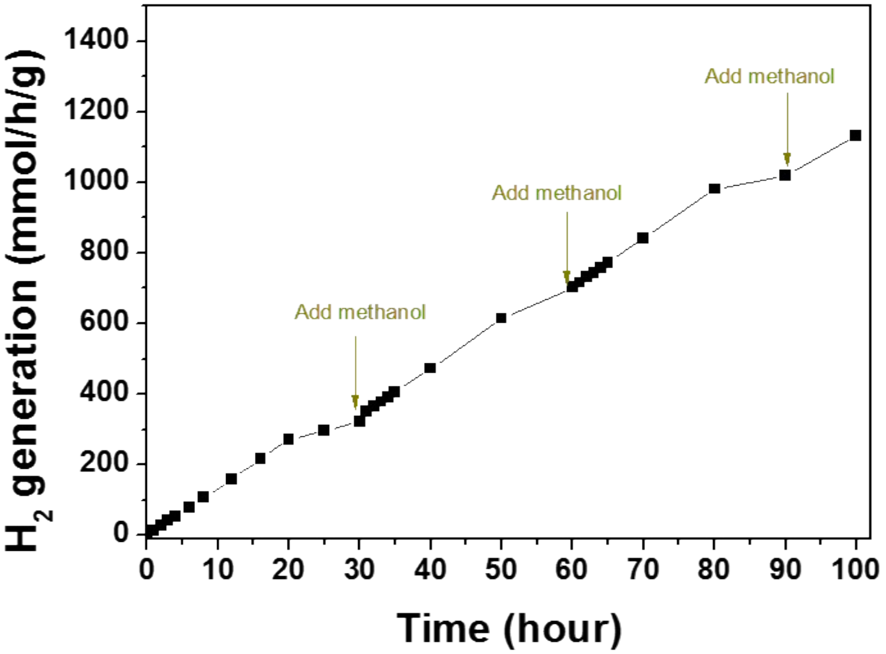

Figure S15. The hydrogen generation of the 0.5 wt.% blue P-25 after 4 days of continuous reaction, the electrolyte of methanol was supplied at 30 hour interval, which exhibits H_2 generation rate of 13.89 mmol/h/g.

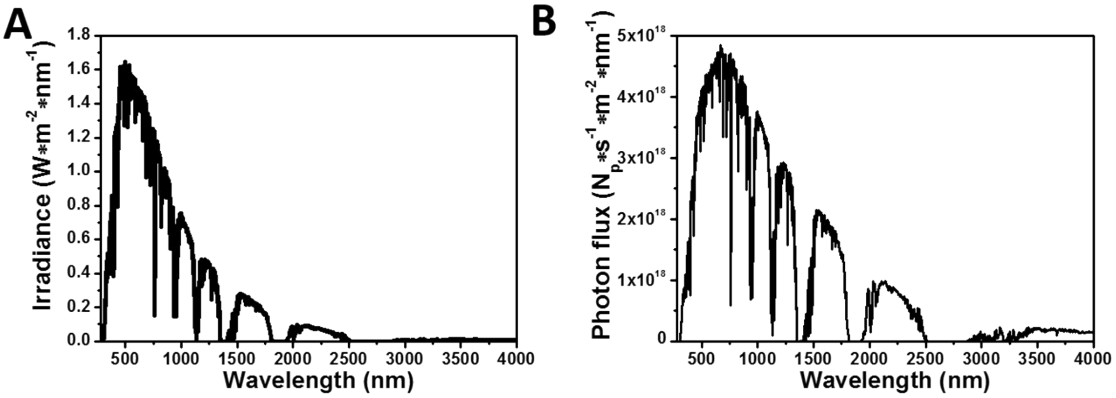

Figure S16. (A) The solar spectral irradiance (AM 1.5G, 100 mW/cm^2). (B) The photon flux converted from the solar spectral irradiance.

References:

1. G. Kresse, *et al.*, Efficient iterative schemes for ab initio total-energy calculations using a plane-wave basis set. *Phys. Rev. B* **54**, 11169–11186 (1996).
2. G. Kresse, *et al.*, Efficiency of ab-initio total energy calculations for metals and semiconductors using a plane-wave basis set. *Comp. Mater. Sci.* **6**, 15–50 (1996).
3. J. P. Perdew, *et al.*, Generalized Gradient Approximation Made Simple. *Phys. Rev. Lett.*, **77**, 3865 (19 96).
4. P. Blöchl, Projector augmented-wave method. *Phys. Rev. B* **50**, 17953–17979 (1994).
5. J. Neugebauer, *et al.*, Adsorbate-substrate and adsorbate-adsorbate interactions of Na and K adlayers on Al(111). *Phys. Rev. B* **46**, 16067 (1992).
6. Stumm, W. Chemistry of the solid water interface. (John Wiley & Sons, Inc.: New York, 1992).
7. Stumm, W. & Morgan, J. J. Aquatic Chemistry. (John Wiley & Sons, Inc.: New York, 1996).
8. J. Pascual, *et al.*, Fine structure in the intrinsic absorption edge of TiO_2. *Phys. Rev. B* **18**, 5606-5614 (1 978).
9. M. Anpo, *et al.*, Eds. Environmentally Benign Photocatalysis-Application of Titanium Dioxide-based Materials; (Springer: New York, 2010).
10. M. Cracker, *et al.*, ^{1}H NMR spectroscopy of titania-chemical shift assignments for hydroxy groups in crystalline and amorphous forms of TiO_2. *J. Chem. Soc. Faraday Trans.* **92**, 2791–2798 (1996).
11. P. Jonsen, *et al.*, Multiple-pulse ^{1}H nuclear magnetic resonance investigations of titania and ruthenium dispersed on titania. *J. Chem. Soc., Faraday Trans.* **87**, 1917–1920 (1991).
12. X. B. Chen, *et al.*, Properties of Disorder-Engineered Black Titanium Dioxide Nanoparticles through Hydrogenation. *Sci. Rep*. **3**, 1510, (2013).
13. D. V. Bavykin, *et al.*, Application of Magic-Angle Spinning NMR to Examine the Nature of Protons in Titanate Nanotubes. *Chem. Mater*. **22**, 2458–2465 (2010).